PHYSICAL REVIEW B **92**, 125113 (2015)

Two-component density functional theory within the projector augmented-wave approach: Accurate and self-consistent computations of positron lifetimes and momentum distributions

Julia Wiktor,[1,*] Gérald Jomard,[1] and Marc Torrent[2]
[1] *CEA, DEN, DEC, Centre de Cadarache, 13108, Saint-Paul-lez-Durance, France*
[2] *CEA, DAM, DIF, F-91297 Arpajon, France*

(Received 21 June 2015; revised manuscript received 18 August 2015; published 8 September 2015)

Many techniques have been developed in the past in order to compute positron lifetimes in materials from first principles. However, there is still a lack of a fast and accurate self-consistent scheme that could handle accurately the forces acting on the ions induced by the presence of the positron. We will show in this paper that we have reached this goal by developing the two-component density functional theory within the projector augmented-wave (PAW) method in the open-source code ABINIT. This tool offers the accuracy of the all-electron methods with the computational efficiency of the plane-wave ones. We can thus deal with supercells that contain few hundreds to thousands of atoms to study point defects as well as more extended defects clusters. Moreover, using the PAW basis set allows us to use techniques able to, for instance, treat strongly correlated systems or spin-orbit coupling, which are necessary to study heavy elements, such as the actinides or their compounds.

DOI: 10.1103/PhysRevB.92.125113 PACS number(s): 31.15.E−, 71.15.Mb, 14.60.Cd, 78.70.Bj

I. INTRODUCTION

Positron annihilation spectroscopy (PAS) has proven to be an efficient nondestructive technique to study defects in materials [1,2]. By measuring the positron lifetime and momentum distribution of annihilating electron-positron pairs one can access information on defects volumes and chemical environments, respectively. However, in order to correctly interpret the experimental data it is often required to compare the measured quantities with calculated ones. The theoretical background of a numerical model that can provide theoretical positron lifetimes and momentum distributions is well known since the 1980s; it is the so-called two-component density functional theory (TCDFT) [1,3,4]. Several implementations of TCDFT have been done and used, however, in most of them the positron wave function is calculated non-self-consistently in an additional run using the electronic densities and effective potential coming from a standard electronic structure calculation [5–9]. Implementations of self-consistent calculations of the positron state have been reported as well [10–13] but they are not distributed. We decided, therefore, to implement TCDFT within the projector augmented-wave (PAW) method in the open-source ABINIT code in a way that allows self-consistent calculations of energies and forces.

This paper is organized as follows: In Sec. II we recall the theory behind the two-component density functional theory and the projector augmented-wave method. We also derive the expressions for energies, positron lifetimes, and momentum distribution in the PAW framework. In Sec. III we present the practical implementation of the described methods. Finally, in Sec. IV we present results of the positron lifetime and momentum distribution calculations that have been performed to validate the implementation.

II. THEORY

A. Two-component density functional theory

In order to calculate the lifetime of a positron and the Doppler broadening of the annihilation radiation, one needs to determine electronic and positronic densities and wave functions in the considered system. These quantities can be computed in the two-component density functional theory (TCDFT) [1,3,4], which is a generalization of the density functional theory.

The total energy in the TCDFT can be written as:

$$\begin{aligned}E[n^+,n^-] = {} & E[n^+] + E[n^-] \\ & + \int d\mathbf{r}\, v_{\text{ext}}(\mathbf{r})[n^-(\mathbf{r}) - n^+(\mathbf{r})] \\ & - \int d\mathbf{r} \int d\mathbf{r}' \frac{n^-(\mathbf{r})n^+(\mathbf{r})}{|\mathbf{r}-\mathbf{r}'|} + E_{\text{c}}^{\text{e-p}}[n^+,n^-],\end{aligned} \tag{1}$$

with $E[n^+]$ and $E[n^-]$, which are the one-component functionals for positron and electrons, v_{ext} is an external potential, and $E_{\text{c}}^{\text{e-p}}$ is an electron-positron correlation functional. It is worth noting that in the above expression both electron and positron densities are positive, while the signs of the external potential acting on the positron and of the electron-positron Hartree interaction are negative.

The momentum distribution of annihilation electron-positron pairs can be written as [1]:

$$\rho(\mathbf{p}) = \pi r_e^2 c \sum_i \left| \int d\mathbf{r}\, e^{-i\mathbf{p}\cdot\mathbf{r}} \Psi_i^{\text{e-p}}(\mathbf{r}) \right|^2, \tag{2}$$

where $\Psi_i^{\text{e-p}}$ is the two-particle wave function in the state i and $\mathbf{p}$ is the given momentum, r_{e} is the classical electron radius, and c is the speed of light. If we consider that the electron and positron are independent [in the independent particle model (IPM)] we can rewrite $\Psi_i^{\text{e-p}}$ as a product of the electronic and positronic wave functions:

$$\Psi_i^{\text{e-p}} = \Psi^+(\mathbf{r})\Psi_i^-(\mathbf{r}). \tag{3}$$

---

[*] julia.wiktor@cea.fr

To take into account the correlation effects between the electrons and positron, one can introduce the position-dependent enhancement factor $\sqrt{g(n^-,n^+)}$ [14], corresponding to the increase in annihilation due to the screening of the positron by the electrons. It is worth noting that often the enhancement factor that depends only on the electronic density is considered and expressed as $\sqrt{\gamma(n^-)}$. However, in this study, we will also use the forms depending on both electron and positron densities. Including the enhancement factor leads to the expression

$$\rho(\mathbf{p}) = \pi r_e^2 c \sum_{ij} \left| \int d\mathbf{r}\, e^{-i\mathbf{p}\cdot\mathbf{r}} \Psi_i^+(\mathbf{r}) \Psi_j^-(\mathbf{r}) \sqrt{g(n^-,n^+)} \right|^2, \quad (4)$$

which is used in the state-independent scheme of momentum distribution calculations.

The positron lifetime, can be calculated as the inverse of the total annihilation rate, which can be obtained by integrating $\rho(\mathbf{p})$ over the momentum:

$$\lambda = \frac{1}{\tau} = \frac{1}{(2\pi)^3} \int d\mathbf{p}\, \rho(\mathbf{p}). \quad (5)$$

On the other hand, the annihilation rate can be also calculated using the electron and positron densities $n^-(\mathbf{r})$ and $n^+(\mathbf{r})$,

$$\lambda = \pi r_e^2 c \int d\mathbf{r}\, n^-(\mathbf{r}) n^+(\mathbf{r}) g(n^-,n^+). \quad (6)$$

Besides using the state-independent scheme, the momentum distribution can be also calculated in the state-dependent scheme [15]. According to Makkonen *et al.* [5] the correlation effects in the state-independent scheme are overestimated, since the enhancement factor $\sqrt{\gamma(n^-)}$ describes the distortion of the electron-positron wave function due to the short-range screening, while the wave function is distorted in whole space. The state-dependent scheme uses a constant enhancement factor γ_j for each electronic state described by the index j. In the state-dependent scheme the momentum distribution is expressed as

$$\rho(\mathbf{p}) = \pi r_e^2 c \sum_{ij} \gamma_j \left| \int d\mathbf{r}\, e^{-i\mathbf{p}\cdot\mathbf{r}} \Psi_i^+(\mathbf{r}) \Psi_j^-(\mathbf{r}) \right|^2, \quad (7)$$

where $\gamma_j = \lambda_j / \lambda_j^{\mathrm{IPM}}$. λ_j is the total annihilation rate calculated for the electronic state j,

$$\lambda_j = \pi r_e^2 c \int d\mathbf{r}\, n_j^-(\mathbf{r}) n^+(\mathbf{r}) \gamma(n^-), \quad (8)$$

and λ_j^{IPM} is the annihilation rate calculated for the same state within the IPM, hence using $\gamma = 1$. When the formulation of the enhancement factor depending on both electron and positron densities $g(n^-,n^+)$ is used, the above expression will be replaced by:

$$\lambda_j = \pi r_e^2 c \int d\mathbf{r}\, n_j^-(\mathbf{r}) n^+(\mathbf{r}) g(n^-,n^+), \quad (9)$$

Makkonen *et al.* [5] showed that the Doppler spectra calculated using the state-independent scheme are in slightly better agreement with the experimental measurements, while the state-dependent scheme overestimates the distribution for high momenta. However, they point out that when ratios of Doppler spectra to a reference spectrum is considered the state-dependent scheme yields better results. As usually the comparison with experiments is made using Doppler spectra ratios and parameters extracted from them, we decided to implement and use the state-dependent scheme.

When determining the electron and positron wave functions and densities needed to calculate the momentum distribution of annihilation radiation and the positron lifetime, one can choose various formulations of electron-positron correlation energy [$E_c^{\mathrm{e-p}}$ in Eq. (1)]. This leads to the existence of several calculations schemes. In the first, conventional scheme (CONV) a LDA zero-positron density limit of the electron-positron correlation functional parametrized for the positron density tending to zero (zero-positron-density limit) is used. This functional was parametrized by Boroński and Nieminen [4] using the data provided by Arponen and Pajanne [16]. In this method it is considered that the positron cannot affect the electronic density, hence only two calculation steps are performed: In the first one the ground-state electronic structure is computed. Then, in the second step, the positron density is calculated for the resulting effective potential and the calculation is stopped. In this method, an enhancement factor depending on the electron density only is used. The CONV scheme, despite being non-self-consistent and considering that the positron density is close to zero even in the case of vacancies, proved to yield results in agreement with experiments [5,17–20]. The second scheme, in which the same parametrization as in CONV is used, but in which the electron and positron densities are calculated self-consistently, was proposed by Gilgien, Galli, Gygi, and Car [21] and is called GGGC. The third scheme, called PSN, uses a full LDA electron-positron correlation functional provided by Puska, Seitsonen, and Nieminen [22] and an enhancement factor depending on both the electron and the positron densities. This scheme was based on the Boroński and Nieminen method [4].

B. Projector augmented-wave method essentials

In this subsection we will recall briefly the basic concepts of the PAW formalism [23] that are necessary to understand how we will apply it in the two-component DFT context. These concepts will only be presented with a view to reemploy them for the electrons-positron system. We will closely stick to the notations introduced in Ref. [24] describing in detail how the PAW method is implemented in the ABINIT package.

In the PAW formalism the Kohn-Sham wave functions Ψ_{nk} are connected to the pseudo-wave-functions $\tilde{\Psi}_{nk}$ by means of the linear transformation:

$$|\Psi_{nk}\rangle = |\tilde{\Psi}_{nk}\rangle + \sum_i \langle \tilde{p}_i | \tilde{\Psi}_{nk} \rangle (|\phi_i\rangle - |\tilde{\phi}_i\rangle). \quad (10)$$

The global index i is used to identify a set of partial waves located at different sites (usually atomic positions). It is a shorthand for the site $\mathbf{R}_i$, the angular momentum quantum numbers (l_i,m_i) and an additional index defining the size of the basis set. The partial waves ϕ_i form a basis of atomic orbitals while the $\tilde{\phi}_i$ are "pseudized" partial waves obtained from ϕ_i—without any norm-conservation constraint—and the $\tilde{p}_i$ are projectors, dual functions of the $\tilde{\phi}_i$.

Starting from Eq. (10) it is possible to show that the total charge density of the electrons can be rewritten as:

$$n(\mathbf{r}) = \tilde{n}(\mathbf{r}) + n^1(\mathbf{r}) - \tilde{n}^1(\mathbf{r}) + n_{\mathrm{c}}(\mathbf{r}), \tag{11}$$

with n_{c} being the density of the frozen-core electrons, which is kept constant and equal to the core density of the isolated atom and

$$\begin{aligned}
\tilde{n}(\mathbf{r}) &= \sum_{nk} f_{nk} \langle \tilde{\Psi}_{nk} | \mathbf{r} \rangle \langle \mathbf{r} | \tilde{\Psi}_{nk} \rangle \\
n^1(\mathbf{r}) &= \sum_{ij} \rho_{ij} \langle \phi_i | \mathbf{r} \rangle \langle \mathbf{r} | \phi_j \rangle \\
\tilde{n}^1(\mathbf{r}) &= \sum_{ij} \rho_{ij} \langle \tilde{\phi}_i | \mathbf{r} \rangle \langle \mathbf{r} | \tilde{\phi}_j \rangle .
\end{aligned} \tag{12}$$

In the above expressions, f_{nk} are the occupation factors of the Kohn-Sham wave functions while the ρ_{ij} scalars are the occupancies of each (i,j) channel and defined as $\rho_{ij} = \sum_{nk} f_{nk} \langle \tilde{\Psi}_{nk} | \tilde{p}_i \rangle \langle \tilde{p}_j | \tilde{\Psi}_{nk} \rangle$.

From the decomposition of the density given in Eq. (11) it is possible to get a direct expression for the total energy (the different terms are detailed in Ref. [24] and in Appendix A):

$$E = \tilde{E} + E^1 - \tilde{E}^1. \tag{13}$$

Using the eigenvalues a double-counting expression for the total energy is also available (see Appendix A). Differentiating the energy towards the density operator leads to the expression of the PAW Hamiltonian [25]:

$$\tilde{\mathrm{H}}[n] = -\frac{1}{2}\Delta + \tilde{v}_{\mathrm{eff}} + \sum_{ij} |\tilde{p}_i\rangle \underbrace{(\hat{D}_{ij} + D^1_{ij} - \tilde{D}^1_{ij})}_{D_{ij}} \langle \tilde{p}_j |, \tag{14}$$

with

$$\begin{aligned}
\hat{D}_{ij} &= \sum_{LM} \int d\mathbf{r}\, \tilde{v}_{\mathrm{eff}}(\mathbf{r}) \hat{Q}^{LM}_{ij}(\mathbf{r}) \\
D^1_{ij} &= \langle \phi_i | -\frac{1}{2}\Delta + v^1_{\mathrm{eff}} | \phi_j \rangle \\
\tilde{D}^1_{ij} &= \langle \tilde{\phi}_i | -\frac{1}{2}\Delta + \tilde{v}^1_{\mathrm{eff}} | \tilde{\phi}_j \rangle \\
&\quad + \sum_{LM} \int_{\Omega_{\mathrm{R}}} d\mathbf{r}\, \tilde{v}^1_{\mathrm{eff}}(\mathbf{r}) \hat{Q}^{LM}_{ij}(\mathbf{r})
\end{aligned} \tag{15}$$

and

$$\begin{aligned}
\tilde{v}_{\mathrm{eff}} &= v_{\mathrm{H}}[\tilde{n} + \hat{n} + \tilde{n}_{\mathrm{Zc}}] + v_{\mathrm{xc}}[\tilde{n} + \hat{n} + \tilde{n}_{\mathrm{c}}] \\
v^1_{\mathrm{eff}} &= v_{\mathrm{H}}[n^1 + n_{\mathrm{Zc}}] + v_{\mathrm{xc}}[n^1 + n_{\mathrm{c}}] \\
\tilde{v}^1_{\mathrm{eff}} &= v_{\mathrm{H}}[\tilde{n}^1 + \hat{n} + \tilde{n}_{\mathrm{Zc}}] + v_{\mathrm{xc}}[\tilde{n}^1 + \hat{n} + \tilde{n}_{\mathrm{c}}].
\end{aligned} \tag{16}$$

In the above equations v_{H} and v_{xc} are Hartree and exchange-correlation potentials. $\tilde{n}_{\mathrm{c}}$ is the pseudized core electron charge density, and n_{Zc} and $\tilde{n}_{\mathrm{Zc}}$ are sums of nucleus and core electron charge densities and pseudized densities. $\hat{Q}^{LM}_{ij}(\mathbf{r})$ is an analytical function, defined as in Ref. [24]. $\hat{n}$ is the compensation charge density, which is added to soft charge densities $\tilde{n}$ and $\tilde{n}^1$ to reproduce the correct multipole moment of the all-electron charge density.

C. Two-component density functional theory within PAW formalism

It is straightforward to write the two-component density functional theory in the framework of the PAW formalism, introducing additional superscripts "$-$" and "$+$" in the formulas in order to refer to electron- and positron-related quantities. As in standard TC-DFT the positron is treated as a positive-density particle interacting with a negative potential due to the ions and valence electrons. The positron wave function is referred as Ψ^+.

1. *Energies*

Following these conventions the total energy of the electrons+positron system can be expressed as:

$$E = E^- + E^+ + E^{+-}. \tag{17}$$

E^- is the contribution to total energy coming from the valence electrons and the ions. It has exactly the same expression as in (18) and (19) in Ref. [24] with the addition of superscript $^-$ at each evolving quantity (density, potential, or wave function). E^+ is the contribution to total energy coming from the positron:

$$E^+ = \tilde{E}^+ + E^{1+} - \tilde{E}^{1+}, \tag{18}$$

with

$$\begin{aligned}
\tilde{E}^+ &= \langle \tilde{\Psi}^+ | -\frac{\Delta}{2} | \tilde{\Psi}^+ \rangle - \int d\mathbf{r}\, v_{\mathrm{H}}[\tilde{n}_{\mathrm{Zc}}](\tilde{n}^+ + \hat{n}^+) \\
E^{1+} &= \sum_{ij} \rho^+_{ij} \langle \phi_i | -\frac{\Delta}{2} | \phi_j \rangle - \int_{\Omega_{\mathrm{R}}} d\mathbf{r}\, v_{\mathrm{H}}[n_{\mathrm{Zc}}](n^{1+}) \\
\tilde{E}^{1+} &= \sum_{ij} \rho^+_{ij} \langle \tilde{\phi}_i | -\frac{\Delta}{2} | \tilde{\phi}_j \rangle \\
&\quad - \int_{\Omega_{\mathrm{R}}} d\mathbf{r}\, v_{\mathrm{H}}[\tilde{n}_{\mathrm{Zc}}](\tilde{n}^{1+} + \hat{n}^+)
\end{aligned} \tag{19}$$

and

$$\rho^+_{ij} = \langle \tilde{\Psi}^+ | \tilde{p}_i \rangle \langle \tilde{p}_j | \tilde{\Psi}^+ \rangle. \tag{20}$$

In the above expression, we use the self-interaction correction, as described by Boroński and Nieminen in Ref. [4] (Appendix B). There is, hence, no positron-positron Hartree and exchange-correlation interaction.

The last contribution to total energy E^{+-} is due to interactions between the positron and the electrons:

$$E^{+-} = \tilde{E}^{+-} + E^{1+-} - \tilde{E}^{1+-}, \tag{21}$$

with

$$\begin{aligned}
\tilde{E}^{+-} &= -\int d\mathbf{r}\, v_{\mathrm{H}}[\tilde{n}^- + \hat{n}^- + \tilde{n}_{\mathrm{Zc}}](\tilde{n}^+ + \hat{n}^+) \\
&\quad + E_{\mathrm{c}}[(\tilde{n}^- + \hat{n}^- + \tilde{n}_{\mathrm{c}}),(\tilde{n}^+ + \hat{n}^+)] \\
E^{1+-} &= -\int_{\Omega_{\mathrm{R}}} d\mathbf{r}\, v_{\mathrm{H}}[n^{1-} + n_{\mathrm{Zc}}](n^{1+}) \\
&\quad + E_{\mathrm{c}}[(n^{1-} + n_{\mathrm{c}}),n^{1+}] \\
\tilde{E}^{1+-} &= -\int_{\Omega_{\mathrm{R}}} d\mathbf{r}\, v_{\mathrm{H}}[\tilde{n}^{1-} + \hat{n}^- + \tilde{n}_{\mathrm{Zc}}](\tilde{n}^{1+} + \hat{n}^+) \\
&\quad + E_{\mathrm{c}}[(\tilde{n}^{1-} + \hat{n}^- + n_{\mathrm{c}}),(\tilde{n}^{1+} + \hat{n}^+)].
\end{aligned} \tag{22}$$

2. Positron lifetime

We can represent the expression for the positron lifetime in the PAW formalism, by introducing Eq. (11) into Eq. (6), which leads to the decomposition of the annihilation rate into three terms (see Appendix B):

$$\lambda = \tilde{\lambda} + \lambda^1 - \tilde{\lambda}^1, \tag{23}$$

where

$$\begin{aligned}
\tilde{\lambda} &= \pi r_e^2 c \int d\mathbf{r}\, \tilde{n}^-(\mathbf{r})\tilde{n}^+(\mathbf{r}) g(\tilde{n}^-,\tilde{n}^+) \\
\lambda^1 &= \pi r_e^2 c \int_{\Omega_R} d\mathbf{r}\, n^{1-}(\mathbf{r}) n^{1+}(\mathbf{r}) g(n^{1-},n^{1+}) \\
\tilde{\lambda}^1 &= \pi r_e^2 c \int_{\Omega_R} d\mathbf{r}\, \tilde{n}^{1-}(\mathbf{r})\tilde{n}^{1+}(\mathbf{r}) g(\tilde{n}^{1-},\tilde{n}^{1+}).
\end{aligned} \tag{24}$$

It is worth noting that it is only possible to obtain the above equation if the partial-waves and plane-waves bases are complete, which is an assumption usually done in the PAW formalism. Two ways of calculating the λ^1 and $\tilde{\lambda}^1$ have been implemented in the code, one estimating them on each point of the radial grid (r,θ,ϕ) and the second using a Taylor development of the densities around their spherical parts (see Appendix C for details).

3. Momentum distribution

Since the momentum distribution of the annihilating electron-positron pairs is a sum over the electronic states, we can consider the core and valence contributions separately. In order to obtain a formula for the valence contribution to the momentum distribution in the PAW formalism, we need to write both electron and positron wave functions in the form given in Eq. (10) and introduce it in Eq. (2). If the partial-waves and plane-waves bases are complete we can derive the following expressions (see Appendix D) for the valence and core contributions, respectively:

$$\begin{aligned}
\rho_{vk}(\mathbf{p}) = \pi r_e^2 c \sum_n \Bigg| &\int d\mathbf{r}\, e^{-i\mathbf{p}\cdot\mathbf{r}} \tilde{\Psi}^+(\mathbf{r}) \tilde{\Psi}^-_{nk}(\mathbf{r}) \\
&+ 4\pi \sum_{ij} \langle \tilde{p}_i | \tilde{\Psi}^+ \rangle \langle \tilde{p}_j | \tilde{\Psi}^-_{nk} \rangle \\
&+ \sum_{LM} S_{LM}(\hat{p})(-i)^L \mathcal{G}^{LM}_{l_i m_i l_j m_j} \\
&\times \int dr (\phi_i(r)\phi_j(r) - \tilde{\phi}_i(r)\tilde{\phi}_j(r)) j_L(pr) \Bigg|^2,
\end{aligned} \tag{25}$$

$$\begin{aligned}
\rho_c(\mathbf{p}) = \pi r_e^2 c \sum_{j_c} \Bigg| 4\pi &\sum_i \langle \tilde{p}_i | \tilde{\Psi}^+ \rangle \\
&\times \sum_{LM} S_{LM}(\hat{p})(-i)^L \mathcal{G}^{LM}_{l_i m_i l_{j_c} m_{j_c}}) \\
&\times \int dr\, \phi_i(r)\phi_{j_c}(r) j_L(pr) \Bigg|^2,
\end{aligned} \tag{26}$$

where $S_{lm_i}(\hat{r})$ are the real spherical harmonics, $j_L(pr)$ is the spherical Bessel function and $\mathcal{G}$ are the real Gaunt coefficients $\mathcal{G}^{LM}_{l_i m_i l_j m_j} = \int d\Omega\, S_{l_i m_i}(\hat{r}) S_{l_j m_j}(\hat{r}) S_{LM}(\hat{r})$ (see Ref. [24]).

The valence contribution $\rho_{vk}(\mathbf{p})$ is calculated for each $\mathbf{k}$ point separately, each time resulting in a momentum distribution given on a different grid (shifted by $\mathbf{k}$) in the reciprocal space. In the above expressions we consider that the positron wave function occupies only one band and one $\mathbf{k}$ point (the Γ point).

III. PRACTICAL IMPLEMENTATION

In practice we implemented the TCDFT as a double loop on the electronic and positronic densities: during each subloop, one of the two densities (and Hamiltonians) is kept constant while the other is being converged (see Fig. 1). If the CONV scheme is performed (e.g., for perfect lattice) the calculation is stopped after two subloops, one electronic and one positronic, and the positron lifetime and momentum distribution are calculated. If a self-consistent scheme is used, the electronic and positronic steps are repeated until the convergence criterion is reached. Additionally, forces acting on atoms and stresses, including contributions from the electrons and the positron (see Appendix E), can be calculated and the calculation continued for the new atomic configuration and/or new geometry. To decrease the computational time when atomic relaxation is performed, each new ionic step is started with an electronic calculation taking into account the potential due to the positron from the last calculation, what

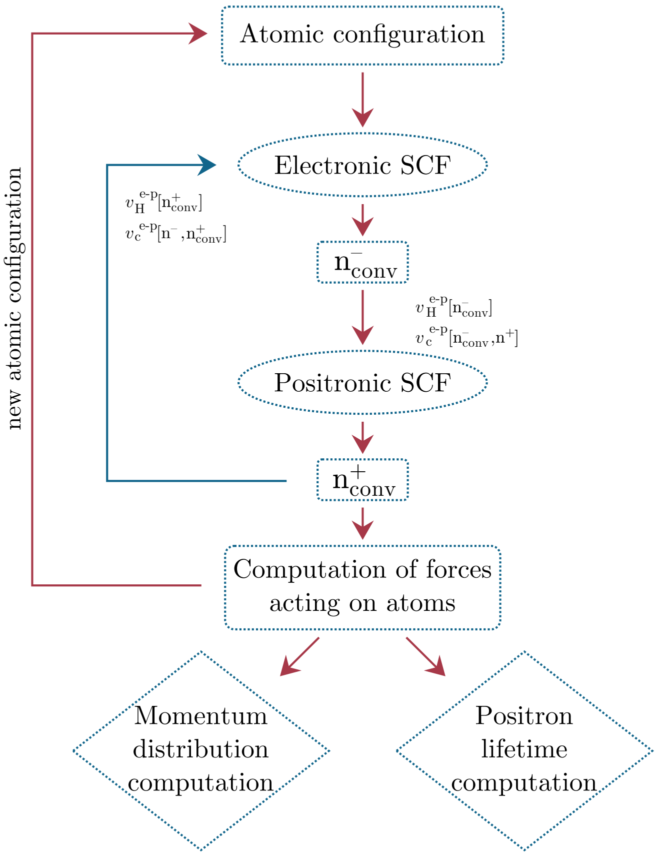

FIG. 1. (Color online) Illustration of the fully self-consistent two-component density functional theory calculations in ABINIT. n^-_{conv} and n^+_{conv} refer to converged electronic and positronic densities, respectively.

can help to decrease significantly the number of iterations. It is worth noting that thanks to the self-consistency and using the same bases for the positron and the electrons we have access to all the force contributions. Therefore, we do not have to make any additional approximations, like it was done for instance in Ref. [5], where atomic-superposition (ATSUP) approximation was used to calculate the positron-induced forces.

In this implementation we use a unified formalism for the positron and the electrons: the wave functions of the electrons and the positron in the system are expressed on the same mixed basis (plane waves and atomic orbitals). Thanks to this, we can use the same PAW data sets for electrons and positron (the sign of the external potential is inverted when the positron is treated), which makes the implementation easy to use.

Several electron-positron correlation functionals have been included and can be used in our implementation:

(i) LDA zero-positron density limit parametrized by Boroński and Nieminen [4] using the data provided by Arponen and Pajanne [16],

(ii) LDA zero-positron density limit fitted by Sterne and Kaiser [26] using the data provided by Arponen and Pajanne [16],

(iii) GGA zero-positron density limit using the gradient correction proposed by Barbiellini *et al.* [27] applied to the LDA parametrization of Boroński and Nieminen [4],

(iv) GGA zero-positron density limit using the gradient correction proposed by Barbiellini *et al.* [27] applied to the LDA parametrization of Sterne and Kaiser [26],

(v) LDA full electron-positron correlation functional provided by Puska, Seitsonen, and Nieminen [22].

If the full electron-positron correlation functional (depending on the positron density) is used, the calculated lifetime of the perfect lattice will depend strongly on the size of the cell. In order to improve the convergence of the lattice lifetime with the cell size, we allow the positron occupation to be set to a value lower than one. This means that a calculation in a one atom cell with the positron occupation set to $1/1000$ will be equivalent to the case of a cell containing 1000 atoms and one positron. The occupations larger than one are not allowed and the positron can only occupy one band.

In the self-consistent calculations, as implemented in this work, we use the same number of $\mathbf{k}$ points in both subloops. This means that, even though the thermalized positron in the lattice should occupy the $\mathbf{k} = 0$ point only, we calculate its density and wave function at all the points that are chosen in the electronic calculation. In the momentum distribution calculations, however, we take only the positron wave function at the Γ point.

The momentum distribution of annihilation radiation can be viewed as a Fourier transform of the product of electrons and positron wave functions. For the plane-wave part of the valence contribution to the momentum distribution [first part of Eq. (25)] this transformation is calculated using fast Fourier transform (FFT) routines as implemented in ABINIT. The grid on which the momentum distribution is calculated is, therefore, equivalent to the grid used for wave functions in the reciprocal space. For each $\mathbf{k}$ point FFT is performed separately, each time giving a result on a different (shifted) grid in the momentum space. The grids are combined at the end of the calculation giving the final momentum grid, whose size is related to the cut-off energy used in the calculation and spacing to the cell size and the $\mathbf{k}$-point mesh. We observed that using a cut-off energy of around 25 Ha is usually sufficient to obtain Doppler spectra converged up to 40 mrad, unless a higher value is needed to converge the total energy of the system. In calculations of the partial valence and core contributions [second part of Eq. (25) and Eq. (26)] we choose to take the $\mathbf{p}$ vectors corresponding to the points of the rectangular grid used for the plane-wave part.

The TCDFT calculations implemented in this work have been parallelized on three levels, allowing one to use the locally optimal block preconditioned conjugate gradient (LOBPCG) [28] or the Chebyshev filtering algorithm [29]. That means that the processors can be distributed between the $\mathbf{k}$ points, bands, and FFT grid points during the density, lifetime, and momentum distribution calculations.

A. Basis completeness

1. *PAW basis completeness for positron wave function*

Deriving the expressions used in TCDFT in the PAW formalism we considered that the PAW basis is complete enough to describe the positron wave function inside the augmentation region. The PAW data sets, however, are generated in order to describe electronic wave functions and not the positronic ones. The nature of the electron-ion and positron-ion interactions and, hence, the shapes of the corresponding wave functions differ strongly. Therefore, in some cases, a standard PAW data set can be inappropriate for the positron description.

In Fig. 2 we illustrate the effect of the choice of the PAW data set on the positron wave function in a Si lattice. The electronic orbitals contained in various data sets used are listed in Table I. First, we used a standard Si PAW data set with four valence electrons ($3s$ and $3p$ basis orbitals)—data set A. With a complete basis we should have $\tilde{\Psi}^{+}(\mathbf{r}) = \sum_i \tilde{\phi}_i(\mathbf{r})\langle \tilde{p}_i|\tilde{\Psi}^{+}\rangle$. However, the corresponding pseudo (PS) and partial pseudo (PS on-site) contributions in Fig. 2(a) are not equal in the augmentation regions. Additionally, we can observe a peak at the (0,0,0) point, which corresponds to the center of a silicon atom, where the positron wave function should be smooth and have its minimum [30,31]. This data set is clearly not appropriate for the positron wave function representation. In Fig. 2(b) we show the positron wave function obtained using a PAW data set with 12 valence electrons ($2s$, $2p$, $3s$, and $3p$ basis orbitals)—data set B. In this case the PS and PS on-site are equal, which means that the basis is complete. There is still a nonzero value of the all-electron wave function at the (0,0,0) point, however, it is much smaller than the one yielded by the four valence electrons data set. It is worth pointing out that we could also enlarge the PAW data set by including projectors corresponding to excited states. However, our test showed that a better description of the positron was always achieved when adding the semicore electron orbitals.

Figure 2 shows clearly that by adding additional states in the PAW data set we obtain a better description of the positron wave function. However, increasing the number of the valence electrons taken into account for a given element leads to more time-consuming calculations. In the cases when large supercells are required (when modeling defects) the computational cost can become too high. We decided to test if

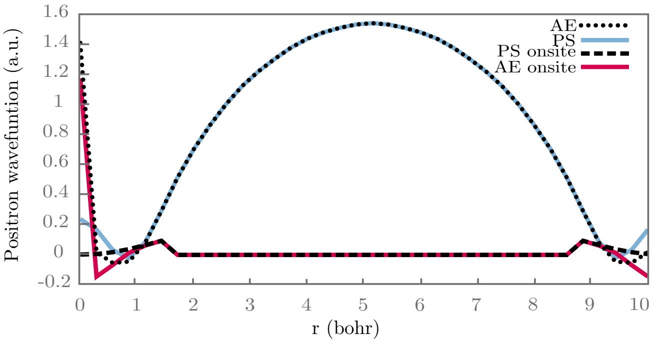

(a) Dataset ‘A’

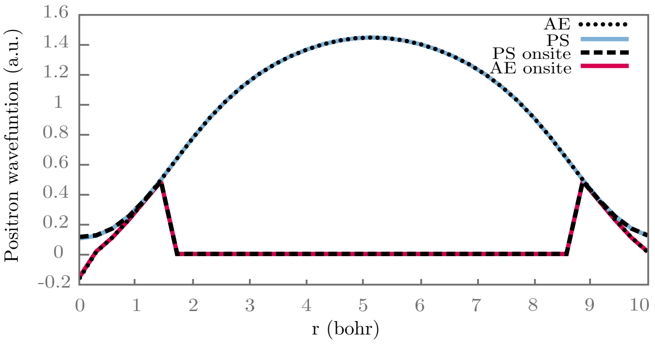

(b) Dataset ‘B’

FIG. 2. (Color online) Positron wave functions in Si lattice obtained using PAW data sets containing four and twelve valence electrons—data sets A and B (see Table I. The wave functions are plotted between two Si atoms at (0,0,0) and (0,0,1) reduced coordinates. All electron (AE), pseudo (PS), partial all electron (AE on-site), and partial pseudo (PS on-site) contributions are presented.

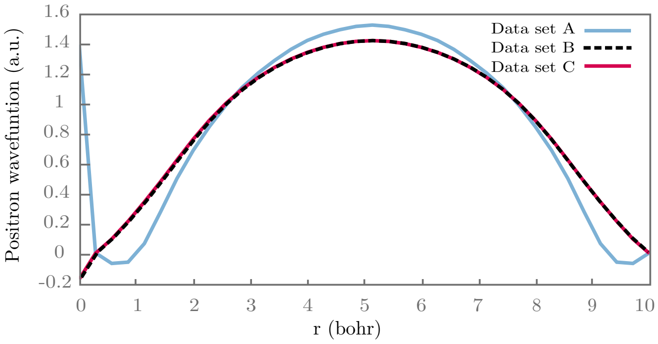

FIG. 3. (Color online) Positron wave functions in a Si lattice obtained using three different PAW data sets, A, B, and C (see Table I). The wave functions are plotted between two Si atoms at (0,0,0) and (0,0,1) reduced coordinates.

it is possible to add the partial waves corresponding to the semicore electrons in the basis used only for the positron wave function description, while keeping the initial number of valence electrons. For instance, in the case of Si, we will still consider four valence electrons, but we will add the $2s$ and $2p$ states in the positron wave function basis. This corresponds to the data set C in Table I. In practice, we generate the PAW data sets (using a modified version of the ATOMPAW generator [32]) in which we add the partial waves and projectors corresponding to these additional states after the standard basis functions. During the self-consistent calculation, when the electronic step is performed, we put to zero all quantities corresponding to these additional states, so that the wave function basis for the electrons is equal to the one calculated with the data set A. This allows us to obtain a better description of the positron wave function without a significant increase of the computational cost. The positron wave function obtained for the Si lattice using the C data set is presented in Fig. 3 and compared with those calculated using data sets A and B. The positron wave functions obtained using data sets B and C are equal, which suggests that both including the semicore electrons in the valence and adding the corresponding states only to the positron wave function basis equally improves the positron description.

TABLE I. Electronic orbitals included in positron and electron basis sets in various PAW data sets used for Si.

Dataset	Orbitals in the positron basis set	Orbitals in the electron basis set
A	$3s$, $3p$	$3s$, $3p$
B	$2s$, $2p$, $3s$, $3p$	$2s$, $2p$, $3s$, $3p$
C	$2s$, $2p$, $3s$, $3p$	$3s$, $3p$

It should be emphasized one more time that the choice of the basis set for the positron wave function description is due to practical and not physical reasons. The positron is described using the electron PAW basis set, to enable the self-consistency and to make the code simple to use. Even though none of the electron wave functions is directly suitable to describe a positron, when a basis set is complete enough, it can describe any function. We did not observe that adding any particular electron state was more efficient in improving the positron description than the other ones (apart from semicore states making reaching the completeness faster than the excited states). In the case of Si described here, we added both s- and p-type functions. We first expected that adding the smooth $2p$ function should be enough to describe the positron, however, it was not the case. Therefore, we believe that the problem is more mathematical than physical and that it is difficult to predict what should be the exact features of the added functions and projectors, apart from making the basis mathematically more complete.

We also tried also to generate basis sets specific to the positron. This did not work, since it was inconsistent with the PAW formalism, which is based on the compensation of the pseudoterms (plane waves and on-site). When using a positron-specific basis set, this compensation was not possible, therefore we believe that the only possibility is to use the same basis for the electrons and the positron. Additionally, we considered adding functions more adapted for the positron description in the positron basis set, as it is done with the semicore states. However, the basis set needs to be orthogonal and during the orthogonalization process these additional functions were transformed to the electron-type functions.

TABLE II. Positron lifetimes for bulk elemental metals in picoseconds. The calculated values are obtained using the CONV scheme. Our results are compared to the work by Takenaka *et al.* using FLAPW [37]. The corresponding experimental values are given in the fourth column.

Material	PAW	FLAPW[a]	Expt.[b]
Li	297	298	291
Al	163	166	163
Fe	100	100	106
Mo	106	104	103
Ag	125	124	133

[a] Reference [37].

[b] Reference [38].

IV. TESTS

A. Positron lifetime

Our implementation of self-consistent calculations of positron lifetimes has been already successfully applied to study defects in silicon carbide [33–35] and uranium dioxide [36]. In Ref. [33] we also included tests performed for Si lattice and monovacancy with a discussion of the partial-waves basis completeness. Here, some additional tests on positron lifetimes will be shown.

1. *Perfect lattices*

In Table II we present the positron lifetime obtained for perfect lattices of elemental metals, compared to the work by Takenaka *et al.* [37] using the all-electron full-potential linearized augmented plane-wave method (FLAPW) and to experimental values. It is worth noting that the FLAPW method is the most accurate implementation of DFT available up to now. The lifetimes calculated using our implementation are in good agreement with the reference ones.

In Table III we present the positron lifetimes calculated for perfect lattices of Si, Al, Cu, and Fe, with and without the semicore electrons (sc. and no sc., respectively). The results are compared with those of Takenaka *et al.* [37]. For Al the positron lifetime is in good agreement with the reference data both with and without the semicore electrons. For Si, Fe, and Cu, however, we can observe the change in the lifetime when the semicore electrons are included. It means that in these cases the partial-waves bases without semicore electrons were not complete enough to describe the positron wave function and density. It is worth stressing that the differences between the results obtained with and without the semicore electrons were mainly due to the description of the positron density as the electronic density was not significantly affected by the choice of the PAW data set.

TABLE III. Positron lifetimes for perfect lattices of Si, Al, Cu, and Fe, with and without the semicore electrons (sc. and no sc., respectively). Results are compared to the work of Takenaka *et al.* [37] using FLAPW. The corresponding experimental values are given in the fourth column.

Material	no sc.	sc.	FLAPW[a]	Expt.
Si	225	209	211	219[b]
Al	162	163	166	163[c]
Fe	97	101	100	106[c]
Cu	123	111	107	110[d]

[a] Reference [37].

[b] Reference [39].

[c] Reference [38].

[d] Reference [40].

TABLE IV. Relative $S_{\rm rel}$ and $W_{\rm rel}$ parameters of silicon monovacancy obtained using different calculations schemes (CONV, GGGC, and PSN). The relaxation, calculated as a percentage of the nearest neighbor distance compared with the ideal vacancy. The positron lifetime calculated using each method is also given.

Scheme	$S_{\rm rel}$	$W_{\rm rel}$	rel. (%)	τ (ps)
CONV unrel.	1.027	0.830	0.0	241
CONV rel.	1.050	0.723	+7.4	264
GGGC	1.046	0.526	+7.4	270
PSN	1.030	0.802	+5.0	272

2. *Vacancy defects*

To test our implementation in the case of defect, we first performed calculations for a silicon monovacancy, using a 216 atom supercell, taking the PAW data set with four valence electrons and $2s$ and $2p$ states added in the positron wave function basis, using three different calculation schemes, CONV, GGGC, and PSN. We performed two different calculations using the CONV scheme, first taking unrelaxed positions and then taking the relaxed positions from the GGGC calculation. This test was performed without the semiconductor correction, hence $1/\epsilon_\infty$ is set to zero in the BN enhancement factor. The results are presented in Table IV. The positron lifetimes obtained with both PSN and GGGC schemes (272 and 270 ps, respectively) are in good agreement with the result obtained by Makkonen *et al.* [5] (272 ps) and with the experimental lifetimes measured by Mäkinen *et al.* (273 ps) [41] and Polity *et al.* (282 ps) [42] for $V_{\rm Si}$.

We also performed a test for a silicon divacancy. Kauppinen *et al.* [43] detected divacancy with a charge -1 and positron lifetime of 300 ps. We performed a calculation in a charged 216 atom supercell, using the PSN scheme and performing a full relaxation. The calculated lifetime of 302 ps is in very good agreement with the experimental value.

B. Momentum distribution

1. *Perfect lattice*

To validate our implementation of the Doppler broadening calculations we compare results obtained using ABINIT to theoretical and experimental spectra presented in literature. Following Makkonen *et al.* [17] we will first compare ratios between spectra of perfect materials. To be able to compare our results to those of Makkonen *et al.* we performed calculations for Si, Al, Fe, and Cu. Additionally, we performed tests for SiC and C in order to be able to make a comparison with ratios of experimental Doppler spectra of diamond, Si and SiC of Rempel *et al.* [44]. We also test our implementation for the

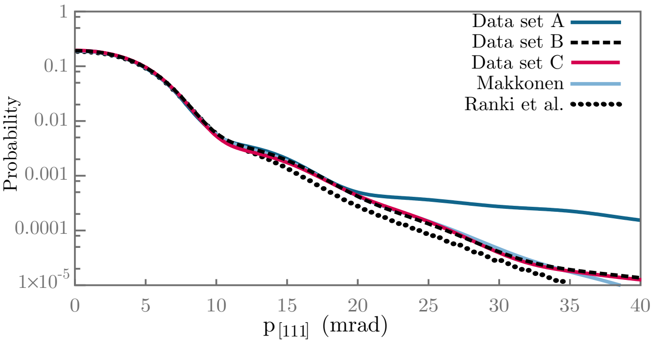

FIG. 4. (Color online) Doppler spectra of Si perfect lattice calculated using three different PAW data sets, A, B, and C (see Table I). Spectra are convoluted with a Gaussian function with a FWHM of 3.7 mrad. The results are compared with a theoretical spectrum given by Makkonen [46] and experimental data obtained by Ranki *et al.* [45].

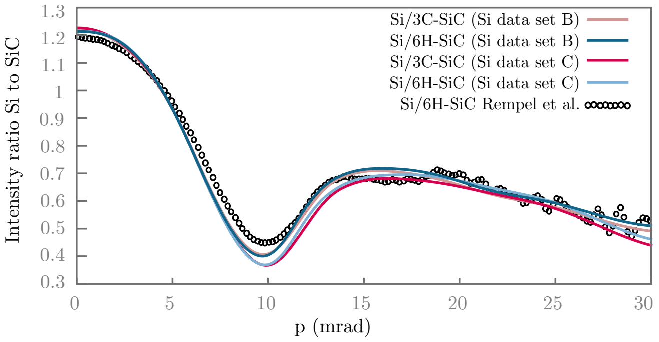

FIG. 5. (Color online) Si lattice/SiC lattice ratio curves of momentum distribution of annihilation radiation. The theoretical results obtained using different silicon PAW data sets are compared with experimental data obtained by Rempel *et al.* [44]. The theoretical curves are convoluted with a Gaussian function with a FWHM of 3.6 mrad.

case of a monovacancy in silicon. In the following tests the calculations results for three different directions, [001], [011] and [111] are averaged, unless stated otherwise.

The first tests have been performed on the perfect lattice of silicon. In this case different PAW data sets containing different number of valence electrons can be used in calculations. These data sets have been discussed in Sec. III A 1. The first data set tested included $3s$ and $3p$ states in the valence and $1s$, $2s$, and $2p$ states in core. The corresponding Doppler spectrum is presented in Fig. 4 (blue line). We can see that the results obtained using this data set are incorrect. We observe an unphysically high probability at high momenta in the spectrum. This is related to the errors in the positron wave function obtained using this data set [see Fig. 2(a)]. In the core region the positron wave function should be smooth and have its minimum [30,31]. Its value at the nucleus should be smaller for heavier elements and can be close to zero already for Na [31]. Meanwhile, in the case of Si, when data set A is used, we observe a peak in the positron wave function in the core region. As a result, for instance, in Eq. (26) we multiply the core contribution by a high value, instead of one tending to zero, which explains the high probability at high momenta. It is worth noting that there was also a nonzero value in the positron wave function calculated using the two more complete data sets, however, the error and the affected region was smaller. We suppose, hence, that the corresponding errors in the Doppler spectrum will appear at momenta above the range that is usually compared with experiments which is around 40 mrad.

The Doppler spectra obtained using the PAW data sets with twelve valence electrons and with four valence electrons and additional $2s$ and $2p$ are presented in black and red, respectively, in Fig. 4. We can see that in both cases the errors at high momenta are suppressed. The spectra are compared with the theoretical results of Makkonen *et al.* and experimental data by Ranki *et al.* [45]. Our results are in very good agreement with those of Makkonen and slightly above the experimental data at higher momenta. The latter is characteristic for the calculations in the state-dependent scheme using the LDA formulation of the enhancement factor [5,15].

The next test consisted of calculating Si lattice/SiC lattice ratio curves (Fig. 5). For Si we used the PAW data sets with twelve valence electrons and four valence electrons and additional $2s$ and $2p$ states. For carbon, we use a data set including all six electrons in valence state. The ratio curves are compared with experimental results of Rempel *et al.* [44]. The theoretical results obtained using both PAW data sets are in very good agreement with the experimental data. In the figure we present the results obtained for both $3C$-SiC and $6H$-SiC. It can be noticed that the momentum distributions of the silicon carbide lattice are very similar for the two polytypes.

We further test our implementation of Doppler broadening calculations in the ABINIT code by repeating some of the tests performed by Makkonen *et al.* in Ref. [17]. In Fig. 6 we plot the Cu lattice to Fe lattice ratio curves of momentum distributions. In this calculation for Cu we used a PAW data set containing 19 valence electrons ($3s$, $3p$, $3d$, $4s$, and $4p$) and $2s$ and $2p$ states added in the positron wave function basis. In the case of Fe we used 16 valence electrons ($3s$, $3p$, $3d$, and $4s$) and $2s$ and $2p$ states added in the positron wave function basis. We compare our ratio curve with theoretical results of Makkonen

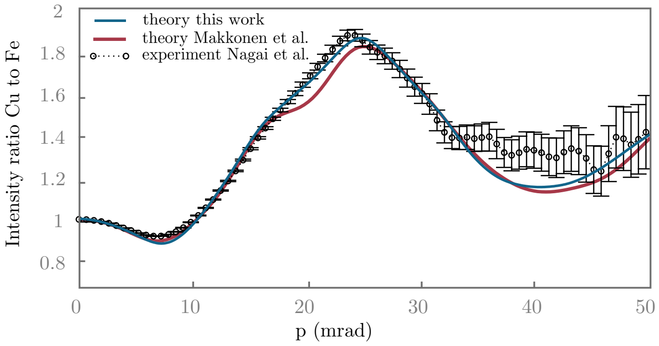

FIG. 6. (Color online) Cu lattice/Fe lattice ratio curves of momentum distributions of annihilation radiation. The result obtained in this study is compared with experimental data obtained by Nagai *et al.* [47] and with theoretical results of Makkonen *et al.* [17]. The theoretical curves are convoluted with a Gaussian function with a FWHM of 4.7 mrad.

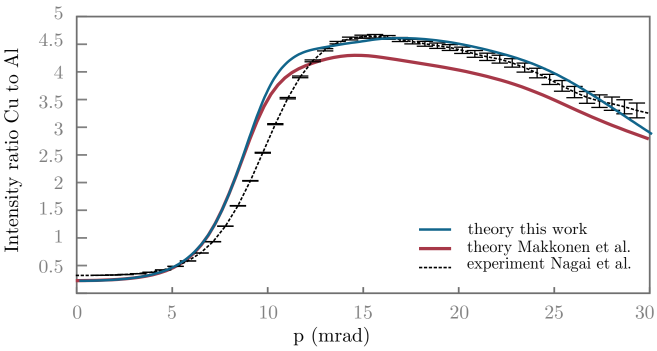

FIG. 7. (Color online) Cu lattice/Al lattice ratio curves of momentum distributions of annihilation radiation. The result obtained in this study is compared with experimental data obtained by Nagai *et al.* [48] and with theoretical results of Makkonen *et al.* [17]. The theoretical curves are convoluted with a Gaussian function with a FWHM of 4.3 mrad.

et al. and experimental data obtained by Nagai *et al.* [47]. The reference results were extracted from Ref. [17]. We can see that our results are in very good agreement with both theoretical and experimental reference data.

In Fig. 7 we plot the Cu lattice to Al lattice ratio curves of momentum distributions. In this calculation we used a PAW data set with 11 valence electrons ($2s$, $2p$, $3s$, and $3p$). In Fig. 8 we plot the Si lattice to Fe lattice and Al lattice to Fe lattice ratio curves. For Si we use the PAW data set with four valence electrons and additional $2s$ and $2p$ states as described previously. We can observe that all the ratio curves obtained using our implementation are in good agreement with the calculations of Makkonen *et al.* and the experimental data of Nagai *et al.* It is worth noting that above 30 mrad the agreement worsens, however, since the relative W parameter that is usually used to describe the high-momentum contribution to the momentum distribution is calculated below that value, this should not be an issue.

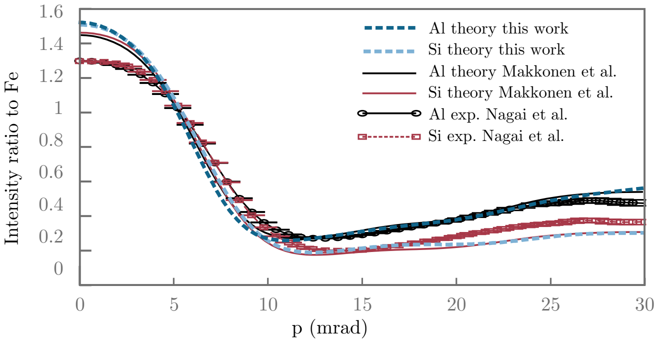

FIG. 8. (Color online) Si lattice/Fe lattice and Al lattice/Fe lattice ratio curves of momentum distributions of annihilation radiation. The result obtained in this study is compared with experimental data obtained by Nagai *et al.* [47] and with theoretical results of Makkonen *et al.* [17]. The theoretical curves are convoluted with a Gaussian function with a FWHM of 4.7 mrad.

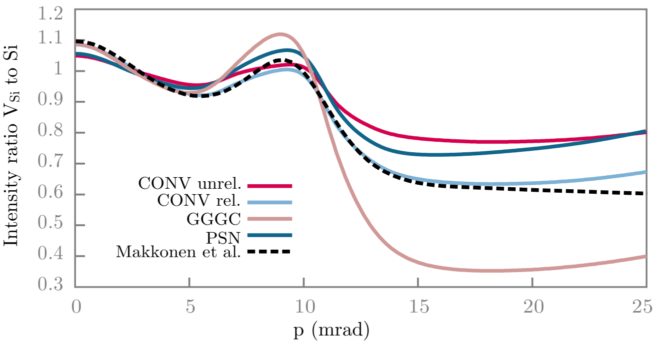

FIG. 9. (Color online) V_{Si}/Si lattice ratio curves of momentum distributions of annihilation radiation in the [001] direction. The results obtained in this study are compared with the results of Makkonen *et al.* [17]. The theoretical curves are convoluted with a Gaussian function with a FWHM of 3.7 mrad.

2. *Vacancy defects*

We test our implementation in the case of a neutral monovacancy and divacancy in Si. We performed calculations using a 216 atom supercell, taking the PAW data set with four valence electrons and $2s$ and $2p$ states added in the positron wave function basis. The results presented in Fig. 9 were obtained using three different calculation schemes, CONV, GGGC and PSN. The vacancy was relaxed using the PSN and GGGC schemes. In the case of the CONV method we performed a calculation first taking unrelaxed positions and then taking the relaxed positions from the GGGC calculation. The results are compared with the results of Makkonen *et al.* [17]. First, we can observe that the low-momentum regions are similar in all calculations and a maximum near 10 mrad is always found. However, the high-momentum parts differ strongly. The GGGC scheme yields the lowest high-momentum ratio, which corresponds to the fact that this scheme overestimates the localization of the positron in the defect and thus predicts a lower positron density in the core region. As in the PSN scheme the positron localization is weaker, the ratio curve obtained using this method is closer to one. The calculation performed for the relaxed monovacancy using the CONV scheme can be compared with the result of Makkonen *et al.*, since they used a similar method in their study. The spectra are in rather good agreement up to 20 mrad, with a slightly higher high-momentum ratio yielded by our calculation. Above 20 mrad the agreement worsens. This can be due to the fact that the methods used in these two calculations are not exactly the same.

In experimental studies, relative $S_{\rm rel}$ and $W_{\rm rel}$ parameters are often considered. In Table IV we present these quantities calculated for silicon monovacancy using the four methods described before. The $S_{\rm rel}$ and $W_{\rm rel}$ parameters were calculated as ratios of vacancy and lattice Doppler spectra in the [001] direction integrated from 0–3 mrad and from 11–20 mrad. We can notice that the $S_{\rm rel}$ and $W_{\rm rel}$ parameters are much more sensitive to the choice of the calculation scheme than the positron lifetimes. The PSN and GGGC methods yield very similar lifetimes for the silicon monovacancy, while the low- and high-momentum contributions to the momentum distribution differ strongly. The fact that the $S_{\rm rel}$

and $W_{\rm rel}$ parameters calculated using the CONV scheme in the unrelaxed configuration and the PSN are very close is most probably a coincidence.

We also performed a test for a negatively charged silicon divacancy, to make a comparison with experimental measurements, since this defect has been observed for instance by Kauppinen *et al.* [43]. We convoluted the spectra with a Gaussian function with a FWHM of 4.7 mrad to mimic the experimental resolution in the reference study and calculated the S and W parameters in ranges from 0–3 mrad and from 11–20 mrad. The $S_{\rm rel}$ and $W_{\rm rel}$ parameters calculated using our implementation and the PSN scheme, 1.050 and 0.72, respectively, are in good agreement with 1.052 ± 0.003 and 0.78 ± 0.02 obtained experimentally. We also performed a calculation for the divacancy using the GGGC scheme, which yielded $S = 1.069$ and $W = 0.476$. These results are in much worse agreement with the experiments. They are also consistent with the trend observed for the monovacancy, where the GGGC method also overestimated low-momentum and underestimated the high-momentum contributions.

V. CONCLUSIONS

We implemented the two-component density functional theory within the projector augmented-wave method (PAW) in the ABINIT package. As opposed to the last implementations of TCDFT of which we are aware, our version allows carrying out fully self-consistent calculations of positron lifetimes and momentum distributions, taking into account the atomic relaxation according to the forces due to electrons as well as the positron. The self-consistent TCDFT calculations in ABINIT can be carried out in a single code run, using the same PAW data set for electrons as well as the positron, which results in an implementation that is easy to use. This tool also allows using several different TCDFT calculation schemes.

In this paper we presented the derivation of expressions for energies, positron lifetime, and momentum distribution of annihilation radiation in the unified PAW formalism used for both the positron and the electrons. It needs to be stressed that the PAW method does not improve the description of the positron wave functions and can even lead to some difficulties in this task. However, we discussed the problem of the partial-waves basis completeness for the positron wave function description and showed that when the PAW data set is carefully chosen and tested, a good description of the positron can be obtained along with positron lifetimes and momentum distributions in good agreement with experimental data. We observed that the partial-waves basis can be extended by both including semicore electrons and by adding the corresponding states as additional functions in the positron basis.

While the inconveniences related to using the PAW method to describe the positron wave function can be easily overcome, this approach has many advantages. It allows one to perform efficient, fully self-consistent TCDFT calculations with an accurate description of the electron wave functions. Using this implementation we can deal with supercells that contain few hundreds to thousands of atoms to study point defects as well as more extended defect clusters. Moreover, using the PAW basis set allows us to use techniques able to, for instance, treat strongly correlated systems or spin-orbit coupling, which are necessary to study heavy elements such as the actinides or their compounds.

ACKNOWLEDGMENTS

The authors are grateful to Ilja Makkonen for fruitful discussions. This research was supported by the basic research program on nuclear materials of the Nuclear Energy Division at CEA, RCOMB. This work was partly performed using HPC resources from GENCI-CCRT (Grant No. x2015096008).

APPENDIX A: VARIOUS EXPRESSIONS FOR THE TOTAL ENERGY

The direct expression of the total energy has the form:

$$E = \tilde{E} + E^1 - \tilde{E}^1 \tag{A1}$$

with

$$\begin{aligned}
\tilde{E} &= \sum_n f_n \langle \tilde{\Psi}_n | -\frac{\Delta}{2} | \tilde{\Psi}_n \rangle + E_{\rm xc}[\tilde{n} + \hat{n} + \tilde{n}_{\rm c}] \\
&\quad + E_{\rm H}[\tilde{n} + \hat{n}] + \int d\mathbf{r}\, v_{\rm H}[\tilde{n}_{Z\rm c}](\tilde{n} + \hat{n}) + U(\mathbf{R}, Z_{\rm ion}) \\
E^1 &= \sum_{ij} \rho_{ij} \langle \phi_i | -\frac{\Delta}{2} | \phi_j \rangle + E_{\rm xc}[n^1 + n_{\rm c}] \\
&\quad + E_{\rm H}[n^1] + \int_{\Omega_{\rm R}} d\mathbf{r}\, v_{\rm H}[n_{Z\rm c}](n^1) \\
\tilde{E}^1 &= \sum_{ij} \rho_{ij} \langle \tilde{\phi}_i | -\frac{\Delta}{2} | \tilde{\phi}_j \rangle + E_{\rm xc}[\tilde{n}^1 + \hat{n} + \tilde{n}_{\rm c}] \\
&\quad + E_{\rm H}[\tilde{n}^1 + \hat{n}] + \int_{\Omega_{\rm R}} d\mathbf{r}\, v_{\rm H}[\tilde{n}_{Z\rm c}](\tilde{n}^1 + \hat{n}).
\end{aligned} \tag{A2}$$

Here, $\tilde{E}$ is the plane-wave contribution to the total energy, while E^1 and $\tilde{E}^1$ are on-site contributions.

It is also possible to write the double counting expression to obtain the energy using the eigenvalues. In this case the total energy takes the form:

$$E = \tilde{E}_{\rm dc} + E^1_{\rm dc} - \tilde{E}^1_{\rm dc} \tag{A3}$$

with

$$\begin{aligned}
\tilde{E}_{\rm dc} &= \sum_n f_n \langle \tilde{\Psi}_n | \tilde{H} | \tilde{\Psi}_n \rangle + E_{\rm xc}[\tilde{n} + \hat{n} + \tilde{n}_{\rm c}] \\
&\quad - \int d\mathbf{r}\, \tilde{v}_{\rm eff}(\tilde{n} + \hat{n}) + U(\mathbf{R}, Z_{\rm ion}) \\
E^1_{\rm dc} &= E_{\rm xc}[n^1 + n_{\rm c}] - \int_{\Omega_{\rm R}} d\mathbf{r} \tilde{v}_{\rm eff}(n^1) \\
\tilde{E}^1_{\rm dc} &= E_{\rm xc}[\tilde{n}^1 + \hat{n} + \tilde{n}_{\rm c}] - \int_{\Omega_{\rm R}} d\mathbf{r}\, \tilde{v}_{\rm eff}(\tilde{n}^1 + \hat{n}).
\end{aligned} \tag{A4}$$

In the above equations all missing definitions can be found in Ref. [24]. It is worth noting that the two expressions for the total energy give exactly the same value, when the density is converged.

APPENDIX B: CALCULATION OF THE POSITRON LIFETIME

Positron lifetime is calculated using positron and electron densities. We can, hence, represent it in the PAW formalism, by introducing Eq. (11) into Eq. (6). In the following we consider that n_c is included in n^{1-} and $\tilde{n}_c$ in $\tilde{n}^-$ and $\tilde{n}^{1-}$. Introducing the PAW formulations of the electron and positron densities, we obtain the expression:

$$\begin{aligned}\lambda = \pi r_e^2 c \int d\mathbf{r}\,([\tilde{n}^-(\mathbf{r}) + n^{1-}(\mathbf{r}) - \tilde{n}^{1-}(\mathbf{r})]\\ + [\tilde{n}^+(\mathbf{r}) + n^{1+}(\mathbf{r}) - \tilde{n}^{1+}(\mathbf{r})]\\ + g(\tilde{n}^- + n^{1-} - \tilde{n}^{1-}, \tilde{n}^+ + n^{1+} - \tilde{n}^{1+})).\end{aligned} \tag{B1}$$

The integral in the above expression can be divided in two parts: the first over the augmentation region and the second outside it, leading to:

$$\begin{aligned}\lambda_{\mathbf{r}\in\Omega_R} = \pi r_e^2 c \int_{\mathbf{r}\in\Omega_R} d\mathbf{r}\,([\tilde{n}^-(\mathbf{r}) + n^{1-}(\mathbf{r}) - \tilde{n}^{1-}(\mathbf{r})]\\ \times [\tilde{n}^+(\mathbf{r}) + n^{1+}(\mathbf{r}) - \tilde{n}^{1+}(\mathbf{r})]\\ \times g(\tilde{n}^- + n^{1-} - \tilde{n}^{1-}, \tilde{n}^+ + n^{1+} - \tilde{n}^{1+}))\end{aligned} \tag{B2}$$

and

$$\begin{aligned}\lambda_{\mathbf{r}\notin\Omega_R} = \pi r_e^2 c \int_{\mathbf{r}\notin\Omega_R} d\mathbf{r}\,([\tilde{n}^-(\mathbf{r}) + n^{1-}(\mathbf{r}) - \tilde{n}^{1-}(\mathbf{r})]\\ \times [\tilde{n}^+(\mathbf{r}) + n^{1+}(\mathbf{r}) - \tilde{n}^{1+}(\mathbf{r})]\\ \times g(\tilde{n}^- + n^{1-} - \tilde{n}^{1-}, \tilde{n}^+ + n^{1+} - \tilde{n}^{1+})).\end{aligned} \tag{B3}$$

Inside the augmentation region, if the partial-waves and plane-waves bases are complete, $\tilde{n} = \tilde{n}^1$ and $\tilde{n}^+ = \tilde{n}^{1+}$, which leads to:

$$\lambda_{\mathbf{r}\in\Omega_R} = \pi r_e^2 c \int_{\mathbf{r}\in\Omega_R} d\mathbf{r}\, n^{1-}(\mathbf{r}) n^{1+}(\mathbf{r}) g(n^{1-}, n^{1+}). \tag{B4}$$

Outside the augmentation region $n^1 - \tilde{n}^1 = 0$ and $n^{1+} - \tilde{n}^{1+} = 0$, which leads to:

$$\lambda_{\mathbf{r}\notin\Omega_R} = \pi r_e^2 c \int_{\mathbf{r}\notin\Omega_R} d\mathbf{r}\,[\tilde{n}^-(\mathbf{r})(\mathbf{r})]\tilde{n}^+(\mathbf{r}) g(\tilde{n}^-, \tilde{n}^+). \tag{B5}$$

Inside the augmentation region we can also write the subtraction of two equal integrals, which will allow as to simplify the expression for the annihilation rate:

$$\begin{aligned}\int_{\mathbf{r}\in\Omega_R} d\mathbf{r}\,\tilde{n}^-(\mathbf{r})\tilde{n}^+(\mathbf{r}) g(\tilde{n}^-, \tilde{n}^+)\\ - \int_{\mathbf{r}\in\Omega_R} d\mathbf{r}\,\tilde{n}^{1-}(\mathbf{r})\tilde{n}^{1+}(\mathbf{r}) g(\tilde{n}^{1-}, \tilde{n}^{1+}) = 0.\end{aligned} \tag{B6}$$

By adding the two integrals from Eq. (B6) to the decomposed λ from Eqs. (B4) and (B5) we obtain:

$$\begin{aligned}\lambda = \pi r_e^2 c \bigg(\int_{\mathbf{r}\notin\Omega_R} d\mathbf{r}\,\tilde{n}^-(\mathbf{r})\tilde{n}^+(\mathbf{r}) g(\tilde{n}^-, \tilde{n}^+)\\ + \int_{\mathbf{r}\in\Omega_R} d\mathbf{r}\,\tilde{n}^-(\mathbf{r})\tilde{n}^+(\mathbf{r}) g(\tilde{n}^-, \tilde{n}^+)\\ + \int_{\mathbf{r}\in\Omega_R} d\mathbf{r}\, n^{1-}(\mathbf{r}) n^{1+}(\mathbf{r}) g(n^{1-}, n^{1+})\\ - \int_{\mathbf{r}\in\Omega_R} d\mathbf{r}\,\tilde{n}^{1-}(\mathbf{r})\tilde{n}^{1+}(\mathbf{r}) g(\tilde{n}^{1-}, \tilde{n}^{1+}) \bigg).\end{aligned} \tag{B7}$$

We can gather the first two integrals and extend the intervals of the last two to the whole space, since they are equal to zero outside the augmentation region. This leads to the final expression for the annihilation rate decomposed in three terms:

$$\lambda = \tilde{\lambda} + \lambda^1 - \tilde{\lambda}^1, \tag{B8}$$

where

$$\begin{aligned}\tilde{\lambda} &= \pi r_e^2 c \int d\mathbf{r}\,\tilde{n}^-(\mathbf{r})\tilde{n}^+(\mathbf{r}) g(\tilde{n}^-, \tilde{n}^+)\\ \lambda^1 &= \pi r_e^2 c \int_{\Omega_R} d\mathbf{r}\, n^{1-}(\mathbf{r}) n^{1+}(\mathbf{r}) g(n^{1-}, n^{1+})\\ \tilde{\lambda}^1 &= \pi r_e^2 c \int_{\Omega_R} d\mathbf{r}\,\tilde{n}^{1-}(\mathbf{r})\tilde{n}^{1+}(\mathbf{r}) g(\tilde{n}^{1-}, \tilde{n}^{1+}).\end{aligned} \tag{B9}$$

Two possible ways of calculating the last terms in the above equation are discussed in Appendix C. The expression for the positron lifetime in the PAW formalism including a compensation charge density $\hat{n}^{1-}(\mathbf{r})$ can be also derived in the same way as presented above. We observed, however, that introducing the compensation charge density has no significant effect on the calculated positron lifetimes. This is consistent with, e.g., the two formalisms for the exchange-correlation functionals in PAW, as described in Ref. [49].

APPENDIX C: CALCULATION OF ON-SITE CONTRIBUTIONS TO ELECTRON-POSITRON ANNIHILATION RATE

Two ways of calculating the PAW on-site contributions to the annihilation rate have been implemented. The first one consists in estimating the two last terms in Eq. (24) [or Eq. (B9)] on each point of a radial grid (r,θ,ϕ). This method is straightforward but requires important computational resources. The other scheme—much more efficient and inspired by the computation of exchange-correlation potential [24]—uses a Taylor development of the densities around their spherical part.

Each on-site density is expanded over the real spherical harmonics, as well as the enhancement factor:

$$n^{1\pm}(\mathbf{r}) = \sum_{LM} n_{LM}^{1\pm}(r) S_{LM}(\hat{r}), \tag{C1}$$

$$g(n^{1-}(\mathbf{r}), n^{1+}(\mathbf{r})) = \sum_{LM} g_{LM}(r) S_{LM}(\hat{r}). \tag{C2}$$

At the second order around the spherically symmetric densities $n^{1s\pm}(\mathbf{r}) = n^{1\pm}_{00}(r)S_{00}(\hat{r})$, the enhancement factor becomes:

$$\begin{aligned} g(n^{1-}(\mathbf{r}),n^{1+}(\mathbf{r})) = {} & g[n^{1s-}(\mathbf{r}),n^{1s+}(\mathbf{r})] + (n^{1-}(\mathbf{r}) - n^{1s-}(\mathbf{r}))\frac{dg}{dn^-}(n^{1s-},n^{1s+}) + (n^{1+}(\mathbf{r}) - n^{1s+}(\mathbf{r}))\frac{dg}{dn^+}(n^{1s-},n^{1s+}) \\ & + \frac{(n^{1-}(\mathbf{r}) - n^{1s-}(\mathbf{r}))^2}{2}\frac{d^2g}{d^2n^-}(n^{1s-},n^{1s+}) + \frac{(n^{1+}(\mathbf{r}) - n^{1s+}(\mathbf{r}))^2}{2}\frac{d^2g}{d^2n^+}(n^{1s-},n^{1s+}) \\ & + [n^{1-}(\mathbf{r}) - n^{1s-}(\mathbf{r})][n^{1+}(\mathbf{r}) - n^{1s+}(\mathbf{r})] \times \frac{d^2g}{dn^-dn^+}(n^{1s-},n^{1s+}). \end{aligned} \tag{C3}$$

Then, after some straightforward manipulations, we obtain the spherical moments of the enhancement factor

$$g_{LM}(r) = \int_{\Omega_R} d\Omega\, g[n^{1-}(\mathbf{r}),n^{1+}(\mathbf{r})]S_{LM}(\hat{r}), \tag{C4}$$

$$\begin{aligned} g_{00}(r) = {} & \sqrt{4\pi}\, g[n^{1s-}(r),n^{1s+}(r)] + \frac{1}{2\sqrt{4\pi}}\frac{d^2g}{d^2n^-}[n^{1s-}(r),n^{1s+}(r)]\sum_{L'M'\rangle 0}[n^{1-}_{L'M'}(r)]^2 + \frac{1}{2\sqrt{4\pi}}\frac{d^2g}{d^2n^+}(n^{1s-(r)},n^{1s+}(r)) \\ & \times \sum_{L'M'\rangle 0}\left[n^{1+}_{L'M'}(r)\right]^2 + \frac{1}{\sqrt{4\pi}}\frac{d^2g}{dn^-dn^+}[n^{1s-}(r),n^{1s+}(r)] \times \sum_{L'M'\rangle 0}\left[n^{1-}_{L'M'}(r)n^{1+}_{\mathrm{L'M'}}(r)\right], \end{aligned} \tag{C5}$$

$$\begin{aligned} g_{LM\rangle 0}(r) = {} & \frac{dg}{dn^-}[n^{1s-}(r),n^{1s+}(r)]n^{1-}_{LM}(r) + \frac{dg}{dn^+}[n^{1s-}(r),n^{1s+}(r)]n^{1+}_{LM}(r) + \frac{1}{2}\frac{d^2g}{d^2n^-}[n^{1s-}(r),n^{s+}(r)] \\ & \times \sum_{L'M'\rangle 0}\sum_{L''M''\rangle 0} n^{1-}_{L'M'}(r)n^{1-}_{L''M''}(r)\mathcal{G}^{LM}_{L'M'L''M''} + \frac{1}{2}\frac{d^2g}{d^2n^+}[n^{1s-}(r),n^{1s+}(r)] \\ & \times \sum_{L'M'\rangle 0}\sum_{L''M''\rangle 0} n^{1+}_{L'M'}(r)n^{1+}_{L''M''}(r)\mathcal{G}^{LM}_{L'M'L''M''} + \frac{d^2g}{dn^-dn^+}[n^{1s-}(r),n^{1s+}(r)] \\ & \times \sum_{L'M'\rangle 0}\sum_{L''M''\rangle 0} n^{1-}_{L'M'}(r)n^{1+}_{L''M''}(r)\mathcal{G}^{LM}_{L'M'L''M''}. \end{aligned} \tag{C6}$$

The on-site contribution to the total annihilation rate is finally given by:

$$\begin{aligned} \lambda^1 &= \int_{\Omega_R} d\mathbf{r}\sum_{LM} n^{1-}_{LM}(r)S_{LM}(\hat{r})\sum_{L'M'} n^{1+}_{L'M'}(r)S_{L'M'}(\hat{r}) \times \sum_{L''M''} g_{L''M''}(r)S_{L''M''}(\hat{r}) \\ &= \sum_{LM}\sum_{L'M'}\sum_{L''M''}\mathcal{G}^{LM}_{L'M'L''M''} \times \int dr n^{1-}_{LM}(r)n^{1+}_{L'M'}(r)g_{L''M''}(r). \end{aligned} \tag{C7}$$

To get the annihilation rate on-site contributions, it is only necessary to know $g[n^{1s-}(r),n^{1s+}(r)]$ and its two first derivatives on the one-dimensional radial grid. The derivatives can be computed via a finite differences scheme, as already done for the exchange-correlation potential [24].

APPENDIX D: CALCULATION OF THE MOMENTUM DISTRIBUTION

1. Valence electrons

The first step towards expressing the valence contribution to the momentum distribution of the annihilating electron-positron pairs in the PAW formalism is to implement the PAW form of the electron and positron wave functions into Eq. (4). The product of electron and positron wave functions needed in this equation takes the form:

$$\Psi^+(\mathbf{r})\Psi^-_{nk}(\mathbf{r}) = \left(\tilde{\Psi}^+(\mathbf{r}) + \sum_i(\phi_i(\mathbf{r}) - \tilde{\phi}_i(\mathbf{r}))\langle\tilde{p}_i|\tilde{\Psi}^+\rangle\right) \times \left(\tilde{\Psi}^-_{nk}(\mathbf{r}) + \sum_j(\phi_j(\mathbf{r}) - \tilde{\phi}_j(\mathbf{r}))\langle\tilde{p}_j|\tilde{\Psi}^-_{nk}\rangle\right). \tag{D1}$$

Multiplication of the terms in the brackets leads to:

$$\begin{aligned} \Psi^+(\mathbf{r})\Psi^-_{nk}(\mathbf{r}) = {} & \tilde{\Psi}^+(\mathbf{r})\tilde{\Psi}^-_{nk}(\mathbf{r}) + \tilde{\Psi}^+(\mathbf{r})\sum_j(\phi_j(\mathbf{r}) - \tilde{\phi}_j(\mathbf{r}))\langle\tilde{p}_j|\tilde{\Psi}^-_{nk}\rangle + \tilde{\Psi}^-_{nk}(\mathbf{r})\sum_i(\phi_i(\mathbf{r}) - \tilde{\phi}_i(\mathbf{r}))\langle\tilde{p}_i|\tilde{\Psi}^+\rangle \\ & + \sum_{ij}\phi_i(\mathbf{r})(\phi_j(\mathbf{r}) - \tilde{\phi}_j(\mathbf{r}))\langle\tilde{p}_i|\tilde{\Psi}^+\rangle\langle\tilde{p}_j|\tilde{\Psi}^-_{nk}\rangle - \sum_{ij}\tilde{\phi}_i(\mathbf{r})(\phi_j(\mathbf{r}) - \tilde{\phi}_j(\mathbf{r}))\langle\tilde{p}_i|\tilde{\Psi}^+\rangle\langle\tilde{p}_j|\tilde{\Psi}^-_{nk}\rangle. \end{aligned} \tag{D2}$$

By definition, outside the augmentation region the wave function is equal to the pseudo part only, hence $\phi_j(\mathbf{r}) - \tilde{\phi}_j(\mathbf{r})$ is equal to zero. Inside the augmentation region, on the other hand, if the basis is complete, $\tilde{\Psi}^+(\mathbf{r}) = \sum_i\tilde{\phi}_i(\mathbf{r})\langle\tilde{p}_i|\tilde{\Psi}^+\rangle$ and

$\tilde{\Psi}^-(\mathbf{r}) = \sum_j \tilde{\phi}_j(\mathbf{r})\langle\tilde{p}_j|\tilde{\Psi}^-\rangle$. We can rewrite the products of quantities existing in the whole space and those that have nonzero values only inside the augmentation region as:

$$\tilde{\Psi}^+(\mathbf{r})\sum_j(\phi_j(\mathbf{r}) - \tilde{\phi}_j(\mathbf{r}))\langle\tilde{p}_j|\tilde{\Psi}^-_{nk}\rangle = \sum_{ij}\tilde{\phi}_i(\mathbf{r})(\phi_j(\mathbf{r}) - \tilde{\phi}_j(\mathbf{r}))\langle\tilde{p}_i|\tilde{\Psi}^+\rangle\langle\tilde{p}_j|\tilde{\Psi}^-_{nk}\rangle \tag{D3}$$

and

$$\tilde{\Psi}^-_{nk}(\mathbf{r})\sum_i(\phi_i(\mathbf{r}) - \tilde{\phi}_i(\mathbf{r}))\langle\tilde{p}_i|\tilde{\Psi}^+\rangle = \sum_{ij}\tilde{\phi}_j(\mathbf{r})(\phi_i(\mathbf{r}) - \tilde{\phi}_i(\mathbf{r}))\langle\tilde{p}_i|\tilde{\Psi}^+\rangle\langle\tilde{p}_j|\tilde{\Psi}^-_{nk}\rangle. \tag{D4}$$

This leads to:

$$\Psi^+(\mathbf{r})\Psi^-_{nk}(\mathbf{r}) = \tilde{\Psi}^+(\mathbf{r})\tilde{\Psi}^-_{nk}(\mathbf{r}) + \sum_{ij}(\phi_i(\mathbf{r})\phi_j(\mathbf{r}) - \tilde{\phi}_i(\mathbf{r})\tilde{\phi}_j(\mathbf{r}))\langle\tilde{p}_i|\tilde{\Psi}^+\rangle\langle\tilde{p}_j|\tilde{\Psi}^-_{nk}\rangle, \tag{D5}$$

therefore

$$\rho_{\mathbf{k}}(\mathbf{p}) = \pi r_e^2 c\sum_n\left|\int d\mathbf{r}\, e^{-i\mathbf{p}\cdot\mathbf{r}}\tilde{\Psi}^+(\mathbf{r})\tilde{\Psi}^-_{nk}(\mathbf{r}) + \int d\mathbf{r}\, e^{-i\mathbf{p}\cdot\mathbf{r}}\sum_{ij}(\phi_i(\mathbf{r})\phi_j(\mathbf{r}) - \tilde{\phi}_i(\mathbf{r})\tilde{\phi}_j(\mathbf{r}))\times\langle\tilde{p}_i|\tilde{\Psi}^+\rangle\langle\tilde{p}_j|\tilde{\Psi}^-_{nk}\rangle\right|^2. \tag{D6}$$

We can see that inside the squared modulus above, we obtain a sum of two separate integrals: one containing the pseudo wave functions and one containing partial waves. We can consider each of them separately.

We can further transform the second integral in Eq. (D6). By separating the partial waves into angular and radial parts we obtain

$$\phi_i(\mathbf{r}) = \frac{\phi_i(r)}{r}S_{l_i m_i}(\hat{r}) \tag{D7}$$

and

$$\tilde{\phi}_j(\mathbf{r}) = \frac{\tilde{\phi}_j(r)}{r}S_{l_j m_j}(\hat{r}), \tag{D8}$$

where $S_{LM}(\hat{r})$ are the real spherical harmonics. We can also express the exponential $e^{-i\mathbf{p}\cdot\mathbf{r}}$ as:

$$e^{-i\mathbf{p}\cdot\mathbf{r}} = 4\pi\sum_{LM}(-i)^L S_{LM}(\hat{p})S_{LM}(\hat{r})j_L(pr). \tag{D9}$$

Separation of the angular and radial parts of the second integral from Eq. (D6), using $d\mathbf{r} = r^2 dr d\Omega$, leads to:

$$\begin{aligned}&\int d\mathbf{r}\, e^{-i\mathbf{p}\cdot\mathbf{r}}\sum_{ij}(\phi_i(\mathbf{r})\phi_j(\mathbf{r}) - \tilde{\phi}_i(\mathbf{r})\tilde{\phi}_j(\mathbf{r}))\langle\tilde{p}_i|\tilde{\Psi}^+\rangle\langle\tilde{p}_j|\tilde{\Psi}^-_{nk}\rangle\\ &\quad = 4\pi\sum_{ij}\langle\tilde{p}_i|\tilde{\Psi}^+\rangle\langle\tilde{p}_j|\tilde{\Psi}^-_{nk}\rangle\sum_{LM}S_{LM}(\hat{p})(-i)^L\times\left(\int d\Omega\, S_{l_i m_i}(\hat{r})S_{l_j m_j}(\hat{r})S_{LM}(\hat{r})\right)\\ &\qquad\times\left(\int dr\,\big(\phi_i(r)\phi_j(r) - \tilde{\phi}_i(r)\tilde{\phi}_j(r)\big)j_L(pr)\right).\end{aligned} \tag{D10}$$

By introducing the real Gaunt coefficients $\mathcal{G}$ (see Ref. [24]),

$$\mathcal{G}^{LM}_{l_i m_i l_j m_j} = \int d\Omega\, S_{l_i m_i}(\hat{r})S_{l_j m_j}(\hat{r})S_{LM}(\hat{r}), \tag{D11}$$

we finally obtain the expression

$$\begin{aligned}&\int d\mathbf{r}\; e^{-i\mathbf{p}\cdot\mathbf{r}}\sum_{ij}(\phi_i(\mathbf{r})\phi_j(\mathbf{r}) - \tilde{\phi}_i(\mathbf{r})\tilde{\phi}_j(\mathbf{r}))\langle\tilde{p}_i|\tilde{\Psi}^+\rangle\langle\tilde{p}_j|\tilde{\Psi}^-_{nk}\rangle\\ &\quad = 4\pi\sum_{ij}\langle\tilde{p}_i|\tilde{\Psi}^+\rangle\langle\tilde{p}_j|\tilde{\Psi}^-_{nk}\rangle\sum_{LM}S_{LM}(\hat{p})(-i)^L\times\mathcal{G}^{LM}_{l_i m_i l_j m_j}\int dr\,(\phi_i(r)\phi_j(r) - \tilde{\phi}_i(r)\tilde{\phi}_j(r))j_L(pr).\end{aligned} \tag{D12}$$

2. Core electrons

The contribution of the core electrons to the momentum distribution can be calculated independently to the valence contribution, since each state is treated separately. The core momentum distribution is expressed as:

$$\rho_{\mathrm{c}}(\mathbf{p}) = \pi r_e^2 c \sum_{j_{\mathrm{c}}} \left| \int d\mathbf{r}\, e^{-i\mathbf{p}\cdot\mathbf{r}} \Psi^{+}(\mathbf{r}) \Psi^{-}_{j_{\mathrm{c}}}(\mathbf{r}) \right|^2. \tag{D13}$$

We will express the positron wave function in the PAW formalism, and for the core electrons, we will assume that the core electrons are unaffected by the crystal formation and their wave functions are equal to those of the isolated atom (frozen core approximation),

$$\Psi^{-}_{j_{\mathrm{c}}}(\mathbf{r}) = \phi_{j_{\mathrm{c}}}(\mathbf{r}). \tag{D14}$$

This leads to the following form of the core contribution to the momentum distribution:

$$\rho_{\mathrm{c}}(\mathbf{p}) = \pi r_e^2 c \sum_{j_{\mathrm{c}}} \left| \int d\mathbf{r}\, e^{-i\mathbf{p}\cdot\mathbf{r}} \times \left(\tilde{\Psi}^{+}(\mathbf{r}) + \sum_i (\phi_i(\mathbf{r}) - \tilde{\phi}_i(\mathbf{r})) \langle \tilde{p}_i | \tilde{\Psi}^{+} \rangle \right) \phi_{j_{\mathrm{c}}}(\mathbf{r}) \right|^2. \tag{D15}$$

We will further consider that the core electron wave functions are contained inside the augmentation region. This approximation seems reasonable in the majority of considered cases and can be easily verified. If the pseudopartial waves $\tilde{\phi}_i(\mathbf{r})$ form a complete basis for the pseudo-wave-function $\tilde{\Psi}^{+}(\mathbf{r})$ we have:

$$\int d\mathbf{r}\, e^{-i\mathbf{p}\cdot\mathbf{r}} \left(\tilde{\Psi}^{+}(\mathbf{r}) - \sum_i \langle \tilde{p}_i | \tilde{\Psi}^{+} > \tilde{\phi}_i(\mathbf{r}) \right) \phi_{j_{\mathrm{c}}}(\mathbf{r}) = 0, \tag{D16}$$

which leads to:

$$\rho_{\mathrm{c}}(\mathbf{p}) = \pi r_e^2 c \sum_{j_{\mathrm{c}}} \left| \int d\mathbf{r}\, e^{-i\mathbf{p}\cdot\mathbf{r}} \sum_i \langle \tilde{p}_i | \tilde{\Psi}^{+} \rangle \phi_i(\mathbf{r}) \phi_{j_{\mathrm{c}}}(\mathbf{r}) \right|^2. \tag{D17}$$

Further, we separate the partial waves into angular and radial parts and transform the equations in the same way as it was done for the valence contribution, which leads to the final expression for the core contribution to the momentum distribution:

$$\rho_{\mathrm{c}}(\mathbf{p}) = \pi r_e^2 c \sum_{j_{\mathrm{c}}} \left| 4\pi \sum_i \langle \tilde{p}_i | \tilde{\Psi}^{+} \rangle \sum_{LM} S_{LM}(\hat{p}) (-i)^L \times \mathcal{G}^{LM}_{l_i m_i l_{j_{\mathrm{c}}} m_{j_{\mathrm{c}}}} \int dr\, \phi_i(r) \phi_{j_{\mathrm{c}}}(r) j_L(pr) \right|^2. \tag{D18}$$

APPENDIX E: CALCULATION OF FORCES

From the expression of the TCDFT total energy (1) we can compute the force acting on an atom at position **R**:

$$\mathbf{F}_{\mathbf{R}} = - \left. \frac{\partial E[n^{+}, n^{-}]}{\partial \mathbf{R}} \right|_{\Psi_i} = \mathbf{F}^{-}_{\mathbf{R}} + \mathbf{F}^{+}_{\mathbf{R}} + \mathbf{F}^{+-}_{\mathbf{R}} \tag{E1}$$

with

$$\begin{aligned}
\mathbf{F}^{-}_{\mathbf{R}} &= - \int (\tilde{n}^{-} + \hat{n}^{-})(\mathbf{r}) \frac{\partial v_{\mathrm{H}}[\tilde{n}_{Z\mathrm{c}}]}{\partial \mathbf{R}} d\mathbf{r} - \int v_{\mathrm{xc}}[\tilde{n}^{-} + \hat{n}^{-} + \tilde{n}_{\mathrm{c}}] \frac{\partial \tilde{n}_{\mathrm{c}}}{\partial \mathbf{R}}(\mathbf{r}) d\mathbf{r} \\
&\quad - \sum_{ij} \sum_{nk} f_{nk} (D^{-}_{ij} - \epsilon^{-}_{nk} O_{ij}) \langle \Psi^{-}_{nk} | \frac{\partial |\tilde{p}_i\rangle\langle\tilde{p}_j|}{\partial \mathbf{R}} | \Psi^{-}_{nk} \rangle - \sum_{ij} \rho^{-}_{ij} \int d\mathbf{r} \tilde{v}^{-}_{\mathrm{eff}}(\mathbf{r}) \sum_{LM} \frac{\partial \hat{Q}^{LM}_{ij}(\mathbf{r})}{\partial \mathbf{R}} \\
\mathbf{F}^{+}_{\mathbf{R}} &= \int (\tilde{n}^{+} + \hat{n}^{+})(\mathbf{r}) \frac{\partial v_{\mathrm{H}}[\tilde{n}_{Z\mathrm{c}}]}{\partial \mathbf{R}} d\mathbf{r} - \sum_{ij} (D^{+}_{ij} - \epsilon^{+} O_{ij}) \langle \Psi^{+} | \frac{\partial |\tilde{p}_i\rangle\langle\tilde{p}_j|}{\partial \mathbf{R}} | \Psi^{+} \rangle + \sum_{ij} \rho^{+}_{ij} \int d\mathbf{r} v_{\mathrm{H}}\big[\tilde{n}_{Z\mathrm{c}}\big](\mathbf{r}) \sum_{LM} \frac{\partial \hat{Q}^{LM}_{ij}(\mathbf{r})}{\partial \mathbf{R}} \\
\mathbf{F}^{+-}_{\mathbf{R}} &= - \sum_{ij} \sum_{nk} f_{nk} D^{+-}_{ij} \langle \Psi^{-}_{nk} | \frac{\partial |\tilde{p}_i\rangle\langle\tilde{p}_j|}{\partial \mathbf{R}} | \Psi^{-}_{nk} \rangle - \sum_{ij} D^{-+}_{ij} \langle \Psi^{+} | \frac{\partial |\tilde{p}_i\rangle\langle\tilde{p}_j|}{\partial \mathbf{R}} | \Psi^{+} \rangle \\
&\quad + \sum_{ij} \rho^{+}_{ij} \int d\mathbf{r} v_{\mathrm{H}}[\tilde{n}^{-} + \hat{n}^{-} + \tilde{n}_{Z\mathrm{c}}](\mathbf{r}) \sum_{LM} \frac{\partial \hat{Q}^{LM}_{ij}(\mathbf{r})}{\partial \mathbf{R}}.
\end{aligned} \tag{E2}$$

In the above expression ϵ^{-}_{nk} and ϵ^{+} are the Kohn-Sham eigenvalues of the electrons and the positron and O_{ij} is the overlap matrix (see Ref. [24]). D^{-}_{ij} is defined in Eq. (15), $\tilde{v}^{-}_{\mathrm{eff}}$ is defined in Eq. (16). D^{+}_{ij} D^{+-}_{ij} and D^{-+}_{ij} can be obtained from Eq. (15)

by introducing the electron and positron densities accordingly and inverting the sign of the Hartree potential when necessary. A similar expression to that for the forces can be also derived for the stress tensor.

[1] M. J. Puska and R. M. Nieminen, Rev. Mod. Phys. **66**, 841 (1994).

[2] F. Tuomisto and I. Makkonen, Rev. Mod. Phys. **85**, 1583 (2013).

[3] R. M. Nieminen, E. Boroński, and L. J. Lantto, Phys. Rev. B **32**, 1377 (1985).

[4] E. Boroński and R. M. Nieminen, Phys. Rev. B **34**, 3820 (1986).

[5] I. Makkonen, M. Hakala, and M. J. Puska, Phys. Rev. B **73**, 035103 (2006).

[6] A. Kawasuso, M. Yoshikawa, H. Itoh, R. Krause-Rehberg, F. Redmann, T. Higuchi, and K. Betsuyaku, Physica B **376–377**, 350 (2006).

[7] A. Kawasuso, M. Maekawa, and K. Betsuyaku, J. Phys.: Conf. Ser. **225**, 012027 (2010).

[8] S. Ishibashi, Mater. Sci. Forum **445–446**, 401 (2004).

[9] S. Ishibashi and A. Uedono, J. Phys.: Conf. Ser. **505**, 012010 (2014).

[10] Z. Tang, M. Hasegawa, T. Chiba, M. Saito, A. Kawasuso, Z. Q. Li, R. T. Fu, T. Akahane, Y. Kawazoe, and S. Yamaguchi, Phys. Rev. Lett. **78**, 2236 (1997).

[11] M. Saito and A. Oshiyama, Phys. Rev. B **53**, 7810 (1996).

[12] D. V. Makhov and L. J. Lewis, Phys. Rev. B **71**, 205215 (2005).

[13] S. Ishibashi, J. Phys. Soc. Jpn. **84**, 083703 (2015).

[14] S. Daniuk, G. Kontrym-Sznajd, A. Rubaszek, H. Stachowiak, J. Mayers, P. A. Walters, and R. N. West, J. Phys. F: Met. Phys. **17**, 1365 (1987).

[15] M. Alatalo, B. Barbiellini, M. Hakala, H. Kauppinen, T. Korhonen, M. J. Puska, K. Saarinen, P. Hautojärvi, and R. M. Nieminen, Phys. Rev. B **54**, 2397 (1996).

[16] J. Arponen and E. Pajanne, J. Phys. F **9**, 2359 (1979).

[17] I. Makkonen and M. J. Puska, Phys. Rev. B **76**, 054119 (2007).

[18] A. Calloni, A. Dupasquier, R. Ferragut, P. Folegati, M. M. Iglesias, I. Makkonen, and M. J. Puska, Phys. Rev. B **72**, 054112 (2005).

[19] P. Folegati, I. Makkonen, R. Ferragut, and M. J. Puska, Phys. Rev. B **75**, 054201 (2007).

[20] C. Rauch, I. Makkonen, and F. Tuomisto, Phys. Rev. B **84**, 125201 (2011).

[21] L. Gilgien, G. Galli, F. Gygi, and R. Car, Phys. Rev. Lett. **72**, 3214 (1994).

[22] M. J. Puska, A. P. Seitsonen, and R. M. Nieminen, Phys. Rev. B **52**, 10947 (1995).

[23] P. E. Blöchl, Phys. Rev. B **50**, 17953 (1994).

[24] M. Torrent, F. Jollet, F. Bottin, G. Zérah, and X. Gonze, Comp. Mat. Sci. **42**, 337 (2008).

[25] G. Kresse and D. Joubert, Phys. Rev. B **59**, 1758 (1999).

[26] P. A. Sterne and J. H. Kaiser, Phys. Rev. B **43**, 13892 (1991).

[27] B. Barbiellini, M. J. Puska, T. Korhonen, A. Harju, T. Torsti, and R. M. Nieminen, Phys. Rev. B **53**, 16201 (1996).

[28] F. Bottin, S. Leroux, A. Knyazev, and G. Zérah, Comput. Mater. Sci. **42**, 329 (2008).

[29] A. Levitt and M. Torrent, Comput. Phys. Commun. **187**, 98 (2015).

[30] M. J. Stott and P. Kubica, Phys. Rev. B **11**, 1 (1975).

[31] J. Kuriplach and B. Barbiellini, Phys. Rev. B **89**, 155111 (2014).

[32] N. A. W. Holzwarth, A. R. Tackett, and G. E. Matthews, Comput. Phys. Commun. **135**, 329 (2001).

[33] J. Wiktor, G. Jomard, M. Torrent, and M. Bertolus, Phys. Rev. B **87**, 235207 (2013).

[34] J. Wiktor, G. Jomard, and M. Bertolus, Nucl. Instrum. Meth. **327**, 63 (2014).

[35] J. Wiktor, X. Kerbiriou, G. Jomard, S. Esnouf, M.-F. Barthe, and M. Bertolus, Phys. Rev. B **89**, 155203 (2014).

[36] J. Wiktor, M.-F. Barthe, G. Jomard, M. Torrent, M. Freyss, and M. Bertolus, Phys. Rev. B **90**, 184101 (2014).

[37] H. Takenaka and D. J. Singh, Phys. Rev. B **77**, 155132 (2008).

[38] A. Seeger, F. Banhart, and W. Bauer, in *Positron Annihilation*, edited by L. Dorikens-Vanpraet, M. Dorikens, and D. Segers (World Scientific, Singapore, 1988), pp. 275–277.

[39] B. K. Panda, W. LiMing, S. Fung, and C. D. Beling, Phys. Rev. B **56**, 7356 (1997).

[40] H. E. Schaefer, W. Stuck, F. Banhart, and W. Bauer, Mater. Sci. Forum **15-18**, 117 (1987).

[41] J. Mäkinen, C. Corbel, P. Hautojärvi, P. Moser, and F. Pierre, Phys. Rev. B **39**, 10162 (1989).

[42] A. Polity, F. Börner, S. Huth, S. Eichler, and R. Krause-Rehberg, Phys. Rev. B **58**, 10363 (1998).

[43] H. Kauppinen, C. Corbel, K. Skog, K. Saarinen, T. Laine, P. Hautojärvi, P. Desgardin, and E. Ntsoenzok, Physical Review B **55**, 9598 (1997).

[44] A. A. Rempel, W. Sprengel, K. Blaurock, K. J. Reichle, J. Major, and H.-E. Schaefer, Phys. Rev. Lett. **89**, 185501 (2002).

[45] V. Ranki, A. Pelli, and K. Saarinen, Phys. Rev. B **69**, 115205 (2004).

[46] I. Makkonen, Master's thesis, Helsinki University of Technology, 2004.

[47] Y. Nagai, Z. Tang, and M. Hasegawa, Radiat. Phys. Chem. **58**, 737 (2000).

[48] Y. Nagai, T. Honma, Z. Tang, K. Hono, and M. Hasegawa, Philos. Mag. A **82**, 1559 (2002).

[49] M. Torrent, N. Holzwarth, F. Jollet, D. Harris, N. Lepley, and X. Xu, Comput. Phys. Commun. **181**, 1862 (2010).